11th World Congress on Computational Mechanics (WCCM XI)
5th European Conference on Computational Mechanics (ECCM V)
6th European Conference on Computational Fluid Dynamics (ECFD VI)
E. Oñate, J. Oliver and A. Huerta (Eds)

A THREE-DIMENSIONAL SEMI-ANALYTICAL MODEL FOR PREDICTING OFFSHORE PILE DRIVING NOISE

Q. P. DENG[*†], W. K. JIANG[*], M. TAN[†], J. T. XING[†]

[*] Institute of Vibration, Shock & Noise
Shanghai Jiao Tong University
800 Dongchuan Road, 200240 Shanghai, China
e-mail: wkjiang@sjtu.edu.cn, http://wkjiang.sjtu.edu.cn/EnglishWeb

[†] Fluid Structure Interactions Group, FEE,
University of Southampton, Southampton SO17 1BJ, United Kingdom
email:M.Tan@soton.ac.uk
http://www.southampton.ac.uk/engineering/about/staff/mingyi.page

Key Words: *Under-water noise, Pile driving, Cylindrical shell, Fluid-structure interaction*

Abstract. It radiates high level of wideband underwater noise to drive large tubular piles into the seafloor by hydraulic impact hammers, which may detrimentally impact both fishes and marine mammals, such as dolphins and whales. Noise prediction and reduction are necessary in underwater engineering in order to protect marine animals. This study develops a three-dimensional semi-analytical method, in which the pile is modeled as a thin elastic cylindrical shell, to predict vibrations and underwater acoustic radiations caused by hammer impacts. A modified variational functional based on the Reissner-Naghdi's thin shell theory is proposed to generate the mathematical equations governing the pile-water interactions. The shell is divided into several segments in axial direction, and the sound pressures in both exterior and interior fluid fields are expressed in an analytical series in frequency domain. The soil is modeled as uncoupled springs and dashpots distributed in three directions. The effect of fluid and soil on the pile is taken into consideration by incorporating their virtual works into the variation of the functional. The underwater sound responses in both frequency domain and time domain are obtained. The mechanical model can be used to estimate underwater noise of piling and explore potential noise reduction measures to protect marine animals

1 INTRODUCTION

Pile-driving noise is generally considered to be the most severe underwater noise which

would influence, harm or even kill marine animals inhabiting around piling sites, such as fishes, dolphins and whales [1-3]. Research and prediction on the vibration and sound radiation of the pile draw increasing attention in the academic world. The Finite Element Method (FEM) is a frequently used method for establishing pile-driving models. Axisymmetric FEM models was established to calculate the near-field underwater sound radiation and approximate sound propagation models (parabolic models by Reihall [4] and Kim [5], head wave model by Lippert [6]) were introduced to predict far-field underwater noise. An axisymmetric FEM model is also used by Zampolli to analyze the pile driving noise [7]. Tsouvalas established a semi-analytical model for the prediction of underwater piling noise, in which the shell displacements are expressed in terms of in-vacuo shell eigenmodes and the sound pressure in fluid domain is expressed as analytical functions [8].

This study develops a linear semi-analytical mechanical model based on a modified variational methodology. In this model, the shell displacements are expressed as admissible displacement functions and the fluid pressure is expanded over analytical functions. The model is of advantage in several aspects. Compared with FEM model, the discretization of the fluid volume, the approximate treatment on the truncated artificial boundaries and approximate modeling for sound propagation in far acoustic field are altogether avoided. Compared with the analytical model, the model leads to a solution that is generally easier to obtain than by solving the common differential governing equations directly, because the effort to seek structural eigenfrequencies and eigenmodes is avoided.

Although some simplifications are introduced, the model is effective and efficient in predicting pile-driving noise and gives insights into the pressure distribution in the fluid field in both frequency domain and time domain.

2 MODEL DISCRIPTION

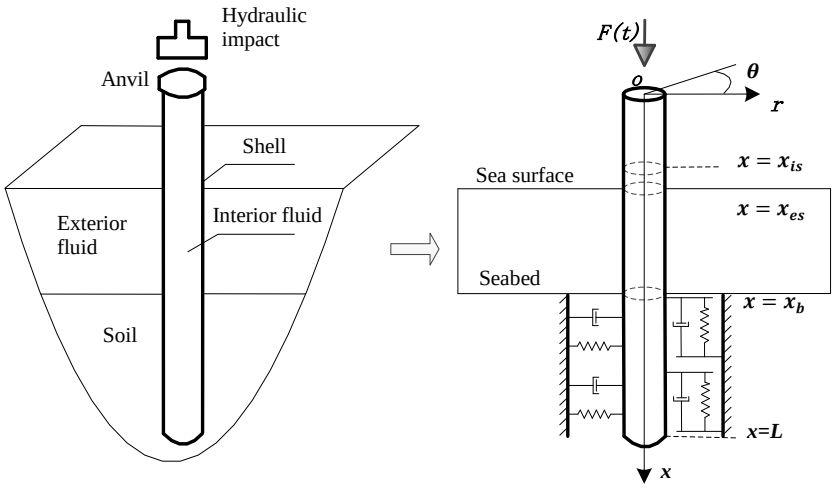

Fig. 1: Pile-driving model

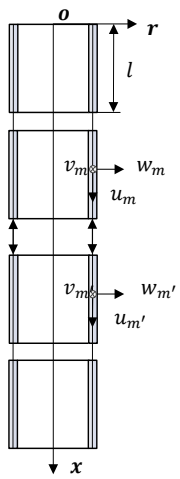

Fig. 2: Pile decomposition

The schematic diagram of the pile-driving model is shown in Fig. 1. A pile is driving into the seabed by a hydraulic impact hammer. The pile is modeled as a thin elastic cylindrical shell of finite length and constant thickness. The hydraulic impact hammer is modeled as a force applied at the top of the pile. The seawater inside and outside the pile is assumed to be incompressible and inviscid. The soil surrounding the pile is modeled as distributed springs and dashpots in three directions along the part of pile ranging over $x_b < x < L$. The fluid-air interface is assumed to be a pressure release boundary, which means sound pressure vanishes on this surface. For the seabed two situations are considered, i.e. a perfectly rigid boundary and a local impedance boundary. The constants $E, \mu, \eta, \rho_s, L, h$ and R correspond to the modulus of elasticity, Poisson ratio, structural loss factor, density, length, thickness and radius of the mid-surface of the cylindrical shell, respectively. c, ρ_f are sound velocity and density of the seawater. The pile is filled by interior fluid at $x_{is} < x < x_b$ and surrounded by exterior fluid at $x_{es} < x < x_b$.

3 BASIC THEORY

A linear 3D semi-analytical mechanical model is established, in which the circular cylindrical tubular pile is divided into several sub-structures along the symmetrical axis. A modified variational methodology is used to establish the governing equations of the system. The displacements of the sub-structures are expressed as summation of a set of admissible displacement functions. The sound pressure in both exterior fluid domain and interior fluid domain is expressed as the summation of a set of analytical functions weighted by the generalized coordinates of the shell displacements. The soil is modeled as uncoupled distributed springs and dashpots in three directions. The coupling effects of both fluid and soil on the pile are taken into consideration by incorporating corresponding work into the total functional of the variational statement. Linear equations in terms of generalized displacement coordinates can be obtained by seeking the stationary state of the total functional.

3.1 Structure decomposition of the pile

A structure decomposition method with high order of accuracy and low computational effort [9, 10] is used here to establish dynamic equations of shell vibration, in which the cylindrical shell is divided into several sub-shells along its axisymmetric axis. As showed in Fig. 2, the shell is decomposed into I sub-shells with equal length l. The method involves seeking the minimum of a modified functional as equation (1). Subscript i is the sub-shell number. T_i and U_i are kinetic energy and strain energy of the sub-shell, respectively. W_i is the work done by external force. $\Pi_{\lambda\kappa}$ is modified energy term incorporated from interface continuity conditions between two adjacent sub-shells. The requirement of interface continuity between two adjacent sub-shells is satisfied by incorporating the terms of continuity constraint conditions $\Pi_{\lambda\kappa}$ into the total energy functional by interface forces and least-squares weighted parameters. This modification on the total energy functional provides a great degree of flexibility for selection of admissible displacement functions, since the interface continuity conditions and geometrical boundary conditions are no longer imposed on the displacement functions, as their eventual satisfaction is implied in the variational

statement. The expressions of kinetic energy T_i, strain energy U_i and work of external force W_i can be found in the authors' previous work [11].

$$\bar{\Pi}_{Tol} = \int_{t_0}^{t_1} \sum_{i=1}^{I} (T_i - U_i + W_i)\, dt + \int_{t_0}^{t_1} \sum_{i,i+1} \Pi_{\lambda\kappa}\, dt \tag{1}$$

The incorporated modified term $\Pi_{\lambda\kappa}$ is given in equation (2). Here $\Theta_u, \Theta_v, \Theta_v, \Theta_v$ are the essential continuity equations on the interface between adjacent cylindrical sub-shells (i) and $(i+1)$, defined as $\Theta_u = u_i - u_{i+1}$, $\Theta_v = v_i - v_{i+1}$, $\Theta_w = w_i - w_{i+1}$, and $\Theta_r = \partial w_i/\partial x - \partial w_{i+1}/\partial x$. $N_x, \bar{N}_{x\theta}, \bar{Q}_x, M_x$ are the resultant force in x direction, circumferential shear resultant force, lateral Kelvin-Kirchhoff shear resultant force and bending moment resultant force on the interface between sub-shells (i) and $(i+1)$, respectively. The function of the first integration term on the right side of equation (2) is to impose a weak enforcement of kinematic interface continuity. As showed in the second integration term on the right side of the equation (2), least-squares weighted residual terms of the continuity equations, i.e. $\Theta_u, \Theta_v, \Theta_v, \Theta_v$, scaled by weighted parameters $\kappa_u, \kappa_v, \kappa_w, \kappa_r$, are incorporated to further modify the total functional. The functional of the least-squares weighted residual terms is to ensure a numerically stable operation for the structure decomposition methodology. The integration corresponding to the essential continuity equations are implemented over the interfaces and geometrical boundary.

$$\begin{aligned} \Pi_{\lambda\kappa} = & \int_0^{2\pi} [N_x\Theta_u + \bar{N}_{x\theta}\Theta_v + \bar{Q}_x\Theta_w - M_x\Theta_r] R d\theta \\ & -\frac{1}{2}\int_0^{2\pi} [\kappa_u\Theta_u^2 + \kappa_v\Theta_v^2 + \kappa_w\Theta_w^2 - \kappa_r\Theta_r^2] R d\theta \end{aligned} \tag{2}$$

3.2 Admissible displacement functions

The displacement components u_i, v_i, w_i in $\bar{\Pi}_{\mathrm{Tol}}$ can be expanded in terms of admissible displacement functions and generalized coordinates. Due to the incorporation of the modified terms, the admissible displacement functions of each sub-shell are not constrained to satisfy any continuity conditions or geometrical boundary conditions. They are only required to be linearly independent, complete and differentiable, which creates considerable flexibility in selection of displacement functions. Compared with analytical method, the effort to seek the in-vacuo shell displacement modes is avoided. Good convergence has been observed when following four kinds of functions are adopted as axial displacement functions [10]: (a) Chebyshev orthogonal polynomials of the first kind; (b) Chebyshev orthogonal polynomials of the second kind; (c) Legendre orthogonal polynomials of the first kind; (d) Hermite orthogonal polynomials [12]. In this model, Fourier series for circumferential expansion and Chebyshev orthogonal polynomials of the first kind for axial expansion are employed as the admissible displacement functions. The displacement components of each sub-shell can be written as equation (3)~(5). $T_m(x)$ is the m^{th} order Chebyshev polynomials. M, N are the highest degrees taken in the polynomials and series, respectively. $\boldsymbol{U}(x,\theta), \boldsymbol{V}(x,\theta), \boldsymbol{W}(x,\theta)$

are admissible displacement function vectors of the three directions. $\boldsymbol{u}_i(t), \boldsymbol{v}_i(t), \boldsymbol{w}_i(t)$ are corresponding generalized coordinate vectors. It should be noted that Chebyshev polynomials are complete and orthogonal series defined on $x \in [-1,1]$ interval while the actual axial coordinate in each sub-shell is defined on $x \in [0, l]$ interval, the coordinate transformations in equation (6) are introduced.

$$u_i(x,\theta,t) = \sum_{m=1}^{M}\sum_{n=0}^{N}\sum_{\alpha=0}^{1} T_m(\bar{x})\cos\left(n\theta + \alpha\frac{\pi}{2}\right)\bar{u}_{mn\alpha}(t) = \boldsymbol{U}(x,\theta)\boldsymbol{u}_i(t) \tag{3}$$

$$v_i(x,\theta,t) = \sum_{m=1}^{M}\sum_{n=0}^{N}\sum_{\alpha=0}^{1} T_m(\bar{x})\sin\left(n\theta + \alpha\frac{\pi}{2}\right)\bar{v}_{mn\alpha}(t) = \boldsymbol{V}(x,\theta)\boldsymbol{v}_i(t) \tag{4}$$

$$w_i(x,\theta,t) = \sum_{m=1}^{M}\sum_{n=0}^{N}\sum_{\alpha=0}^{1} T_m(\bar{x})\cos\left(n\theta + \alpha\frac{\pi}{2}\right)\bar{w}_{mn\alpha}(t) = \boldsymbol{W}(x,\theta)\boldsymbol{w}_i(t) \tag{5}$$

$$x = \frac{l}{2}(\bar{x}+1), \quad \bar{x} = \frac{2}{l}x - 1 \tag{6}$$

3.3 The virtual work of soil

As shown in Fig. 1, the soil is modelled as uniformly distributed elastic springs and dashpots in all directions along the pile wall ranging over $x_b < x < x_L$. The elastic spring and dashpot coefficients are determined in the same manner as described in the previous work [8]. The effect of springs and dashpots on the pile shell is taken into consideration by incorporating their work into the total energy functional $\overline{\Pi}_{Tol}$. The virtual work done by the springs and dashpots can be given as equations (7) and (8). The terms k_x, k_θ, k_r are the soil stiffness and c_x, c_θ, c_r correspond to equivalent viscous soil damping coefficients along the axial, tangential and radial directions, respectively. The term s in the integration is the interface area of the i^{th} sub-shell and surrounding soil. The substitution of soil by uncoupled springs and dashpots is a simplification treatment of the soil effect on the pile. The introduction of springs and dashpots is of practical significance from an engineering point of view, but it throws a challenge in the realistic evaluation of the coefficients and creates uncertainty to the calculations. A detailed analysis of the influence of the spring and dashpot coefficients on sound radiation in exterior fluid domain is referred to [8].

$$\delta W_{ki} = -\int_S (\delta u_i \cdot k_x u_i + \delta v_i \cdot k_\theta v_i + \delta w \cdot k_r w_i) ds, \tag{7}$$

$$\delta W_{ci} = -\int_S \left(\delta u_i \cdot c_x \frac{\partial u_i}{\partial t} + \delta v_i \cdot c_\theta \frac{\partial v_i}{\partial t} + \delta w_i \cdot c_r \frac{\partial w_i}{\partial t}\right) ds, \tag{8}$$

3.4 The virtual work of fluid

In frequency domain, fluid pressure in a circular cylindrical coordinates, with certain regular boundary conditions, can be expanded as a summation of analytical function series by

applying variable separation technique. For the fluid domain outside the pile, the fluid pressure and the velocity component normal to the surface of the shell can be given as equation (9) and (10) [8]. ρ_f is the density of the fluid. $H_n^{(2)}$ is the Hankel function of the second kind and of order n. $H_n'^{(2)}$ denotes its derivative with respect to r. The terms k_{xp}, k_{rp} are wave number in x direction and r direction respectively and they are determined by radian frequency ω and boundary conditions at sea surface and seabed. D_{np} is unknown coefficient which can be determined by normal displacement on structure-fluid coupling interface.

$$\tilde{p}_e(x,r,\theta) = -i\omega\rho_f \sum_{\alpha=0}^{1}\sum_{n=0}^{\infty}\sum_{p=0}^{\infty} D_{np} H_n^{(2)}(k_{rp}r)\sin k_{xp}(x-x_{es})\cos(n\theta+\alpha\frac{\pi}{2}) \tag{9}$$

$$\tilde{v}_{er}(x,r,\theta) = \sum_{\alpha=0}^{1}\sum_{n=0}^{\infty}\sum_{p=0}^{\infty} D_{np} H_n'^{(2)}(k_{rp}r)\sin k_{xp}(x-x_{es})\cos(n\theta+\alpha\frac{\pi}{2}) \tag{10}$$

By making use of the continuity condition on the shell-fluid coupling interfaces, the orthogonality property of fluid modes, the unknown coefficient D_{np} can be obtained. Then the pressure in the exterior fluid domain can be expressed by analytical function series weighted by generalized coordinates of normal displacements, as shown in equation (11).

$$\begin{aligned}\tilde{p}_e(x,r,\theta,\omega) &= \sum_{\alpha=0}^{1}\sum_{n=0}^{\infty}\sum_{i=0}^{I_e}\sum_{p=0}^{\infty}\sum_{m=1}^{M} w_{imn\alpha}\cdot\tilde{P}_{e,inmp\alpha} \quad \text{with:}\\ \tilde{P}_{e,inmp\alpha} &= \frac{\omega^2\rho}{f_p}\frac{H_n^{(2)}(k_{rp}r)}{H_n'^{(2)}(k_{rp}R)}\cdot\sin k_{xp}(x-x_{es})\cdot\cos(n\theta+\alpha\frac{\pi}{2})\\ &\quad\cdot\int_{\bar{x}_i}^{\bar{x}_{i+1}} T_m(x-x_i)\cdot\sin k_{xp}(x-x_{es})\,dx\end{aligned} \tag{11}$$

Use ‘fluid loading’ to describe the effect that the fluid has on the shell vibration [13]. The virtual work done by the exterior fluid pressure on the coupling interface is given as following equation, with superscript ‘*’ denoting the complex conjugate. The derivation procedure of the virtual work of the interior fluid is completely analogous as that of exterior fluid pressure.

$$\delta W_p = \int_0^{2\pi}\int_{x_s}^{x_b} -\delta w_r^*\cdot pR\,dx\,d\theta \tag{12}$$

3.5 Impact force of the hydraulic hammer

The impact force acting on the pile top is modeled as a half sinusoid pulse with a very small duration τ. The impact force is defined as following equation. $F_0(\theta)$ is the peak of the line force distributed on the intersecting line of the middle surface of the shell and cross section on the pile top. For an axisymmetric impact force, $F_d(\theta)$ is independent of θ.

$$F(\theta,t)=\begin{cases}\sin(\pi t/\tau)\int_0^{2\pi}F_0(\theta)d\theta & 0<t<\tau\\ 0 & t<0 \text{ or } t>\tau\end{cases} \tag{13}$$

3.6 Governing equations of the coupling system

Fourier transform pairs with respect to time are introduced herein to transform variables between time domain and frequency domain. By substituting the works done by hydraulic impact force, fluid pressure, spring and dashpot forces into the total functional $\overline{\Pi}_{Tol}$ and performing the variation operation with respect to the generalized coordinate vectors $\boldsymbol{u}$, $\boldsymbol{v}$, $\boldsymbol{w}$, the governing equations of motion of the pile can be obtained as equation (14). $\boldsymbol{M}$ and $\boldsymbol{K}$ are mass matrix and stiffness matrix, respectively. $\overline{\boldsymbol{K}}_{\boldsymbol{\lambda}}$ and $\overline{\boldsymbol{K}}_{\boldsymbol{\kappa}}$ are the generalized interface stiffness matrixes introduced by the interface forces and the least-squares weighted residual parameters, respectively. $\boldsymbol{C_e}$ and $\boldsymbol{C_i}$ are coupling matrixes introduced by fluid pressure in exterior fluid domain and interior fluid domain. $\boldsymbol{C_{soil}}$ is the coupling matrix introduced by soil in contact with the pile. $\boldsymbol{q}(\omega)=[\boldsymbol{u_1^T},\boldsymbol{v_1^T},\boldsymbol{w_1^T},\boldsymbol{u_2^T},\boldsymbol{v_2^T},\boldsymbol{w_2^T},\cdots,\boldsymbol{u_I^T},\boldsymbol{v_I^T},\boldsymbol{w_I^T}]$ is the global generalized coordinate vector of the shell. Response in time domain can be obtained by performing Fourier inverse transformation to frequency response.

$$[-\omega^2\boldsymbol{M}+(\boldsymbol{K}-\overline{\boldsymbol{K}}_{\boldsymbol{\lambda}}+\overline{\boldsymbol{K}}_{\boldsymbol{\kappa}})-\boldsymbol{C_e}+\boldsymbol{C_i}+\boldsymbol{j\omega C_{soil}}]\boldsymbol{q}(\omega)=\boldsymbol{F}(\omega) \tag{14}$$

4 NUMERICAL CASE AND DISCUSSION

Table 1. Model parameters

Part	Parameters
Shell	Geometry: $L=28m, R=1m, h=20mm$
	Material parameters: $E=2.1\times10^{11}, \rho_s=7800kg\ m^{-3}, \mu=0.28, \eta=0.002$
	Decomposition parameters: *M=8*, *I=8*, *N=0*
Fluid	$c=1500m\ s^{-1}, \rho_f=1000kg\ m^{-3},\ x_{es}=10, x_{is}=10, x_b=18$
Soil	$E_{soil}=6\times10^7N\ m^{-1}, \mu_{soil}=0.4, \rho_{soil}=1600kg\ m^{-3}$
	$k_x=6\times10^6N\ m^{-3}, k_\theta=6\times10^6N\ m^{-3}, k_r=1.5\times10^7N\ m^{-3}$
Force	$F_0(\theta)=1\times10^6\ N, \tau=2.5\ ms$

A pile with a certain geometry and material parameters is chosen for numerical case. The seabed is assumed to be perfectly rigid acoustic boundary. The hydraulic impact force is assumed to be uniformly distributed on the circumference of the pile top. The material properties of the shell, geometry and parameters of the model are summarized in Table 1. A reasonable description of the soil should include spring coefficients and dashpot coefficients depending on both exciting frequency and wavelength of the motion of the shell-soil and fluid-soil interfaces. The dashpot coefficients equal the summations of the soil material

damping and radiation damping in corresponding direction. The material damping is expressed with reference to an equivalent damping ratio of the soil throughout the frequency range for a certain strain rate [14]. The radiation damping is introduced to the model in a simple manner as presented in [15]. The spring coefficients are assumed constant throughout the frequency range with average values retrieved from corresponding static stiffness.

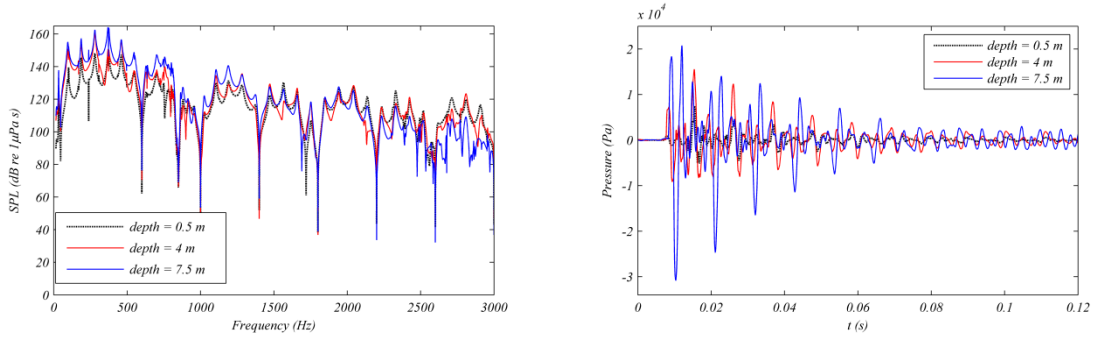

(a) (b)

Fig. 3: Pressure at observed points located 8 m away from the pile surface: (a) SPL frequency spectrum (b) time history

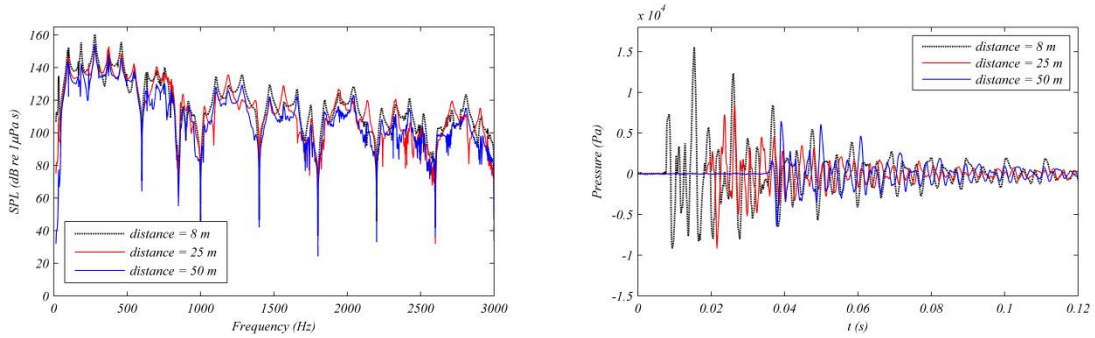

(a) (b)

Fig. 4: Pressure at observed points located 4 m below the sea surface surface: (a) SPL frequency spectrum (b) time history

The frequency spectrums and time histories of sound pressure at three observed points of different depths below the sea surface are shown in Fig. 3. The points are located 8 meters away from the pile surface. It can be seen from Fig. 3 (a) that the sound pressure is depth depedent. Below 1200 Hz, The point close to the seabed has the highest pressure level while the point close to the see surface has the lowest value. In high frequency range, no curve has an obvious dominance over the others. The pressure variation along depth depends on the terms $sin\, k_{xp}(x - x_{es})$ in pressure modes, as given in equation (9). For each mode, a pressure trough emerges on the pressure released boundary and a pressure crest emerges on the rigid seabed. The aforementioned phenomenon in the low frequency range occurs because the upper point is close to the trough while the lower point is close to the crest. As the frequency increases, fluid modes of higher value of k_{xp} and smaller wavelength become dominant. In

high frequency range, the phenomenon no longer exists because the dominant wavelengths become comparative with or even smaller than the distance from the observed points to the adjacent boundaries. The spectrum curves see a downward trend as the frequency increses and experience several sharp troughs. The first trough emerges at $f_1 = 600$ Hz and troughs appear again every 400 Hz along the frequency axis. This is based on the fact that the amplitude of frequency spectrum of the impact force has a downward tendency along frequency axis and vanishes at these corresponding frequencies. The frequencies of the sharp troughs depend on the force duration τ and can be given as $f_i = (1/2 + i)/\tau$.

Fig. 3 (b) shows the time histories of the sound pressures at the three observed points. The pressure curves see their first peaks at about 10 ms and then fluctuates with a rapid attenuation along the time axis. The pressure amplitutes decrese to less than 5000 Pa after 70 ms. The point close to the seabed has the maximum pressure peaks while the point near the sea surface has the minimum values. This is attributed to the fact that the former observed point has the highest and the later one has the lowest pressure amplitute over the low frequency range.

The frequency spectra and time histories of sound pressure of three observed points located 4 m below the sea surface are shown in Fig. 4. The distances from the pile surface to each observed point are 8 m, 25 m and 50 m, respectively. Fig. 4 (a) gives the SPL frequency spectrums of the three points. It is evident that the difference between the three curves is depedent on frequency. The spectrum curve of a nearer observed position is generally higher than that of a farther observed position. A obvious difference between the curves is observed below about 80 Hz and in this frequency range the amplitutes are dramatically small compared with a relatively high frequency range. This phenomenon can be ascribed to presence of evanescent modes. The sound pressure in the exterior fluid field is contributed by both propogating modes and evanescent modes. In this low frequency domain, the exterior sound pressure are mainly contributed by evanescent modes which decrease sharply along the radial direction. Therefore, the pressure in low frequency range nearly vanishes at a distance of 50 m.

The time histories of the pressures at the three points is given in fig. 4 (b). Increase in observed distance leads to both a lag along the time axis and an attentuation in amplitute. An estimated sound propagation speed from the figure is 1500.5 m/s which matches the defined sound speed $c = 1500$ m/s very precisely.

The evolution of the radiated exterior pressure with time for a radial distance up to 16 m is illustrated in Fig. 5. The time step between two adjacent pictures are 2 ms. A compression wave is excited by the impact force at the pile top and prapagates rapidly downwards. When the structural compression wave goes through the fluid field, the fluid is compressed and generates a wave peak which propagates outward along the radial direction. The structural wave in the pile propagates more fast than the sound speed in the fluid, therefore a Mach-cone is formed in the fluid with an angle α with respect to the pile axis. The angle depends on the relationship $\alpha = \tan^{-1}(c/c_s)$ in which c_s is the propagation speed of the compression wave. An estimated value of the angle from the figure is 16.6° whose tangent equals the ratio. The approximate propagation speed of compression wave is 5032 m/s which is slightly smaller

than longitudinal wave velocity in the steel material $c_L = \sqrt{E/\rho} = 5188$ m/s. This phenomenon is also oberved in the previous work [4, 8].

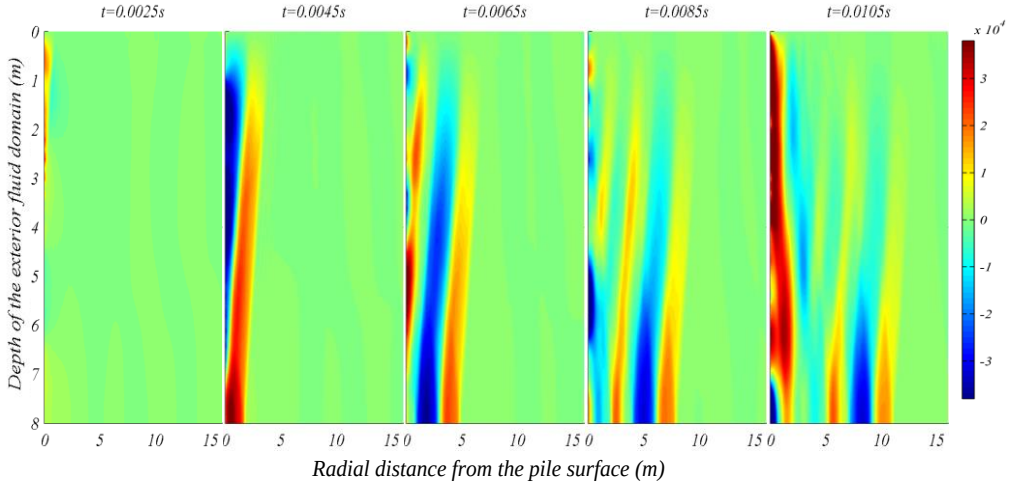

Fig. 5: Pressure in Pa (N/m^2) for time steps starting from 2.5 *ms* to 10.5 *ms*

5 CONCLUSIONS

- A linear semi-analytical method is established for predicting the underwater noise for a pile-water-soil interaction system subject to piling hammer impacts. A modified functional is proposed to derive the numerical equations of the coupled dynamical system, in which the pile is a shell divided into sub-structures, the fluid pressure is expanded by analytical functions and the soil is modeled by uncoupled distributed springs and dashpots.
- The case study reveals that exterior radiated sound pressure is depth-dependent in both frequency domain and time domain. The SPL frequency spectrum of the observed position close to the seabed is obvious higher than that of the position close to the sea surface in the low frequency range. In time domain, higher pressure amplitude is also observed at the point close to seabed.
- The sound pressure attenuates as observed distance increases in both frequency domain and time domain. Sound pressure in the low frequency range is hard to propagate away from the pile due to the dominance of evanescent fluid modes. A Mach-cone is formed in the exterior fluid field as the structural compression wave propagates downward.

ACKNOWLEDGMENT

This work is supported by grant 11272208 of the National Natural Science Foundation of China.

REFERENCES

[1] Madsen, P.T., et al., Wind turbine underwater noise and marine mammals: implications of current knowledge and data needs. *Marine Ecology-Progress Series*, (2006). **309**: p. 279-295.

[2] Slabbekoorn, H., et al., A noisy spring: The impact of globally rising underwater sound levels on fish. *Trends in Ecology and Evolution*, (2010). **25**(7): p. 419-427.

[3] Jefferson, T.A., Hung, S.K., and Wursig, B., Protecting small cetaceans from coastal development: Impact assessment and mitigation experience in Hong Kong. *Marine Policy*, (2009). **33**(2): p. 305-311.

[4] Reinhall, P.G. and Dahl, P.H., Underwater Mach wave radiation from impact pile driving: Theory and observation. *Journal of the Acoustical Society of America*, (2011). **130**(3): p. 1209-1216.

[5] Kim, H., et al., Long range propagation modeling of offshore wind turbine noise using finite element and parabolic equation models. *The Journal of the Acoustical Society of America*, (2012). **131**(4): p. 3392-3392.

[6] Lippert, T., Lippert, S., and Estorff, O.v., PREDICTION OF PILE DRIVING INDUCED UNDERWATER NOISE. *19th International Congress on Sound and Vibration*, (2012).

[7] Zampolli, M., et al., Validation of finite element computations for the quantitative prediction of underwater noise from impact pile driving. *The Journal of the Acoustical Society of America*, (2013). **133**(1): p. 72-81.

[8] Tsouvalas, A. and Metrikine, A.V., A semi-analytical model for the prediction of underwater noise from offshore pile driving. *Journal of Sound and Vibration*, (2013).

[9] Qu, Y.G., et al., Free and forced vibration analysis of uniform and stepped circular cylindrical shells using a domain decomposition method. *Applied Acoustics*, (2013). **74**(3): p. 425-439.

[10] Qu, Y.G., Hua, H.X., and Meng, G., A domain decomposition approach for vibration analysis of isotropic and composite cylindrical shells with arbitrary boundaries. *Composite Structures*, (2013). **95**: p. 307-321.

[11] Deng, Q.P. and Jiang, W.K. *A semi-analytical model for predicting underwater noise radiated from offshore pile driving*. *APCOM & ISCM*, (2013), Singapore.

[12] Jeffrey, A. and Dai, H.H., *Handbook of Mathematical Formulas and Integrals*. 2008: Elsevier Science.

[13] Fahy, F.J. and Gardonio, P., *Sound and Structural Vibration: Radiation, Transmission and Response*. 2007: Elsevier Science.

[14] Gazetas, B.G. and Dobry, R., Horizontal response of piles in layered soils. *Journal of Geotechnical Engineering*, (1984). **110**: p. 937-956.

[15] Gazetas, G. and Dobry, R., Simple Radiation Damping Model for Piles and Footings. *Journal of Engineering Mechanics*, (1984). **110**(6): p. 937.